

Hydrologic cycling over Antarctica during the middle Miocene warming

Sarah J. Feakins^{1*}, Sophie Warny² and Jung-Eun Lee³

From 20 to 15 million years (Myr) ago, a period of global warmth reversed the previous ice growth on Antarctica, leading to the retreat of the West Antarctic Ice Sheet and the contraction of the East Antarctic Ice Sheet^{1,2}. Pollen recovered from the Antarctic shelf indicates the presence of substantial vegetation on the margins of Antarctica 15.7 Myr ago³. However, the hydrologic regime that supported this vegetation is unclear. Here we combine leaf-wax hydrogen isotopes and pollen assemblages from Ross Sea sediments with model simulations to reconstruct vegetation, precipitation and temperature in Antarctica during the middle Miocene. Average leaf-wax stable hydrogen isotope (δD) values from 20 to 15.5 Myr ago translate to average δD values of -50‰ for precipitation at the margins of Antarctica, higher than modern values. We find that vegetation persisted from 20 to 15.5 Myr ago, with peak expansions 16.4 and 15.7 Myr ago coinciding with peak global warmth⁴ and vegetation growth⁵. Our model experiments are consistent with a local moisture source in the Southern Ocean⁶. Combining proxy measurements with climate simulations, we conclude that summer temperatures were about 11°C warmer than today, and that there was a substantial increase in moisture delivery to the Antarctic coast.

Understanding the hydrologic cycle during past times of global warmth and reduced ice cover can provide constraints on the fundamental laws governing the climate system. The middle Miocene represents an intriguing period of Earth history during which high temperatures and a substantial retreat of the West Antarctic Ice Sheet and shrinkage of the East Antarctic Ice Sheet^{1,2}, occurred under CO_2 levels in the range of 190–850 ppmv (refs 7,8). At the height of the middle Miocene Climatic Optimum, global annual mean surface temperatures were $\sim 3^\circ\text{C}$ higher than present, equivalent to projections for the coming century, with 6°C warming in mid latitudes and 10°C warming for high latitudes, based on an evaluation of proxy data and model simulations⁹. As the present warming is already causing melting of Antarctic ice¹⁰, the apparent similarities with the middle Miocene make this a climatic period of profound interest. Here we report multiproxy evidence (pollen concentrations, leaf-wax concentrations and leaf-wax isotopes) from the Antarctic geologic drilling (ANDRILL) programme's AND-2A core in the Ross Sea ($77^\circ 45.488'\text{S}$, $165^\circ 16.613'\text{E}$) recording local warmth and the presence of vegetation around the continental margins (Supplementary Fig. S1). In particular, we use the hydrogen isotopic composition of plant leaf waxes as a tracer of the hydrological cycle during middle Miocene warmth.

It has been suggested that Antarctica was progressively glaciated after 34 Myr ago and vegetation became increasingly restricted to the margins of the continent¹¹. However, recent discoveries from the AND-2A core indicate dynamic conditions in the Antarctic cryosphere between 20 and 10 Myr ago (ref. 12). A sharp increase

in *Nothofagidites* (southern beech) and *Podocarpidites* (podocarp conifer) pollen was linked to the growth of vegetation on Antarctica (Fig. 1a,b), at the same time as evidence for ice-free oceans and fresh water on land (Fig. 1c,d) during a rapid warming event 15.7 Myr ago (ref. 3). Here, we reanalysed an earlier palynomorph peak at finer resolution and identify the largest vegetation expansion of the past 34 Myr, 16.4 Myr ago (Fig. 1a,b and Supplementary Table S1). The temporal distribution of pollen and spores indicates that local vegetation was tundra with small trees growing in protected areas throughout the middle Miocene. This type of vegetation indicates that the climate was somewhat cooler than that found at the modern austral polar-alpine tree limit ($<10^\circ\text{C}$ in the warmest month), which today is best represented in the southerly Chilean Andes. Peak pollen abundance is composed of species present throughout the middle Miocene in lower quantities indicating that these species had expanded from local refugia. Low species diversity and poor dispersal characteristics of many of these taxa confirm that the vegetation expansion during warm intervals was achieved by recolonization from local sources of cold-tolerant, tundra species and not long-range transport³.

Plant leaf waxes identified for the first time in Antarctic margin sediments provide independent evidence for vegetation during the middle Miocene. Peak wax concentrations up to $2.5\text{ }\mu\text{g}$ per gram of dry weight (gdw^{-1} ; Fig. 1e) coincide with peak pollen indicating a coherent signal of vegetation optima. Although plant leaf waxes can be transported thousands of kilometres, they are not ubiquitous in these sediments suggesting that long-range transport is unlikely here. Consideration of both archives suggests that refugia of tundra vegetation survived on the margins of Antarctica throughout the middle Miocene, with increases in primary productivity, pollen production and possibly stature (to more tree-like form) during two optima 15.7 and 16.4 Myr ago.

Hydrogen isotope analysis of these plant leaf waxes offers new insights into climate during the middle Miocene. Stable isotopes in precipitation act as a tracer of the hydrological cycle, with the most depleted values on the planet falling over the isolated, high-elevation East Antarctic Ice Sheet¹³. Isotopic composition is strongly associated with spatial gradients in temperatures in mid and high latitudes¹⁴. On Antarctica the δD values of precipitation and snow covary spatially with temperature, elevation and distance inland¹³. Using observed spatial relationships, temporal variations in temperature have been inferred from Pleistocene ice-core records from the continental interior at Vostok¹⁵ and Dome C extending back to 0.8 Myr ago (ref. 16). There is, unfortunately, no earlier glacial stratigraphy surviving on Antarctica, although subterranean ice has been reported from the dry valleys¹⁷. Plant leaf wax is therefore our best proxy for the hydrogen isotopic composition of precipitation for deep time applications¹⁸. Previous application of this technique to Arctic Palaeocene–Eocene Thermal Maximum

¹University of Southern California, Department of Earth Sciences, Los Angeles, California 90089-0740, USA, ²Louisiana State University, Department of Geology and Geophysics and Museum of Natural Science, Baton Rouge, Louisiana 70803, USA, ³Jet Propulsion Laboratory, California Institute of Technology, Pasadena, California 91109, USA. *e-mail: feakins@usc.edu.

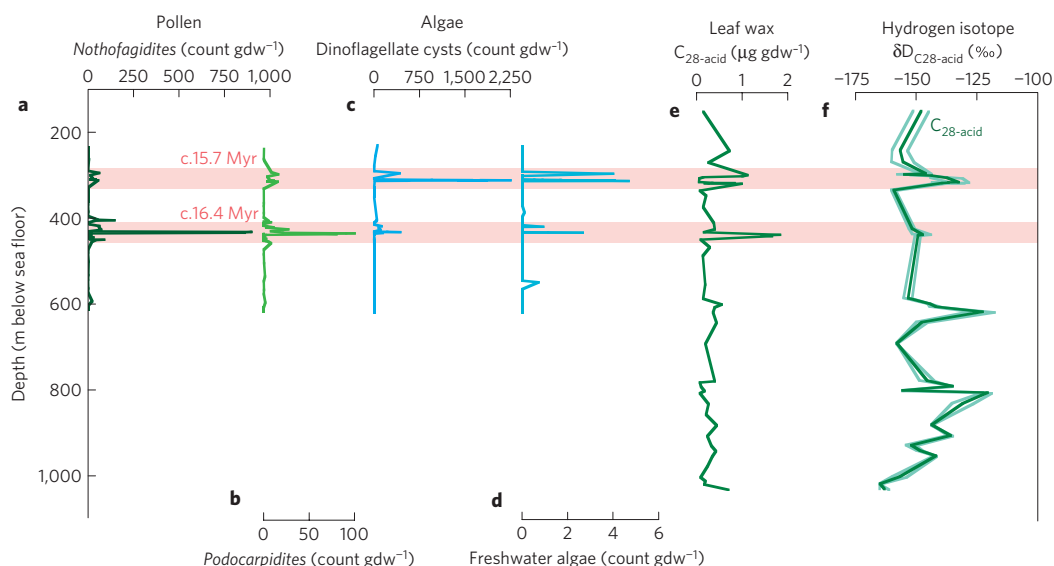


Figure 1 | Geochemical and palynological results from AND-2A core. a, b, Pollen relative abundance and **c,** relative relative abundance of dinocysts produced by dinoflagellate species tolerant of low salinity and **d,** freshwater algae. Data in **a–d** from ref. 3 and this study. **e,** Leaf-wax abundance. **f,** δD , mean (dark green), one standard deviation (light green). These and additional data are provided in table format in the Supplementary Information. Pink shading highlights two peaks identified in abundance data.

(PETM) age deposits has demonstrated striking differences in high northern latitude hydrological conditions during extreme greenhouse conditions 55 Myr ago relative to modern¹⁹.

We identify C_{20} to C_{30} *n*-alkanoic acids (hereafter acid) from the marine sediments of the AND-2A core between 144 and 1,100 m below sea floor, equivalent to 20–10 Myr (ref. 20). *n*-acids with chain lengths longer than C_{24} with a strong even-over-odd chain length predominance are derived from the waxy coating on terrestrial plant leaves, presumably forming during austral summer (December–February). Leaf waxes are transported to marine sediments by fluvial or aeolian transport. Glacial erosion is also a candidate during the re-advance of the East Antarctic Ice Sheet after 14 Myr (ref. 21). The presence of *n*-acids with isotopic variability within the homologous series and between closely spaced samples, indicates that leaf waxes are well preserved and that isotopic composition is unaltered (Supplementary Information).

We select the C_{28} -acid for plant-leaf-wax-based palaeoprecipitation reconstructions as it is sufficiently abundant and most probably derived from terrestrial leaf waxes. δD values of the C_{28} -acid range from -165 to -121 ‰ and average -146 ± 2 ‰ (1 standard error of the mean (s.e.m.), $n = 37$, Fig. 1f and Supplementary Table S2). To calculate palaeoprecipitation, the measured δD values must be adjusted for the net fractionation ($\epsilon_{\text{acid/precip}}$) between precipitation (precip) and leaf-wax *n*-acids. Modern calibration studies, typically on the C_{29} *n*-alkane, indicate $\epsilon_{\text{alkane/precip}} = -121 \pm 2$ ‰ (1 s.e.m., $n = 316$) and must be adjusted for $\epsilon_{\text{alkane/acid}} = 25$ ‰ (ref. 18). Although smaller fractionations have been reported for some species in greenhouse experiments under continuous light²², high-latitude fractionations²³ have not been established as significantly different from the global data set. We therefore assume $\epsilon_{\text{acid/precip}}$ values of -100 ± 2 ‰ (1 s.e.m.) in Miocene palaeoprecipitation predictions, similar to fractionations applied in Eocene reconstructions ($\epsilon_{\text{alkane/precip}} = -140$ ‰ (ref. 24) and -130 to -100 ‰; ref. 19) after correction for compound class. Using these constraints, we calculate that Antarctic coastal palaeoprecipitation averages -51 ± 3 ‰ (compounded 1 s.e.m., Fig. 2 and Supplementary Information).

Modern snow samples across the continent range from -150 to -450 ‰ depending primarily on temperature and distance inland; with coastal, sea level precipitation at 77° S close to the AND-2A site having an approximate δD value of -150 ‰ (ref. 13). In

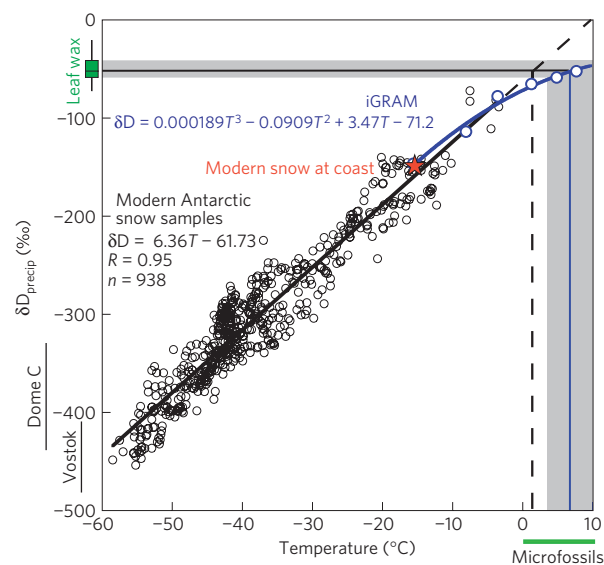


Figure 2 | T– δD relationship for Antarctica comparing modern versus Miocene. Modern snow across Antarctica (black; ref. 13) and locally (red) with spatial slope. Model results (blue) for coast at 77° S using iGRAM by varying atmospheric opacity (Supplementary Fig. S2). Leaf-wax-based Miocene δD_{precip} (green), box and whisker plot showing median (line), 25th and 75th percentiles (rectangle) and range (error bars). Temperature conversion of median value, using extrapolated modern slope (black dashed line), model slope (dark blue) and 25th–75th percentile using model slope (shaded area). Microfossil temperature estimates³ and Pleistocene range of δD_{ice} values from Vostok¹⁵ and Dome C (ref. 16; labelled bars).

contrast, our Miocene δD_{precip} estimates for coastal Antarctica are dramatically heavier than modern (Fig. 2).

This raises questions as to how such isotopically heavy precipitation can fall at the margins of the Antarctic continent during the middle Miocene and what this may mean for the regional and global climate system. Clues originate from microfossil analyses in the same sediments that indicate ice-free conditions in the

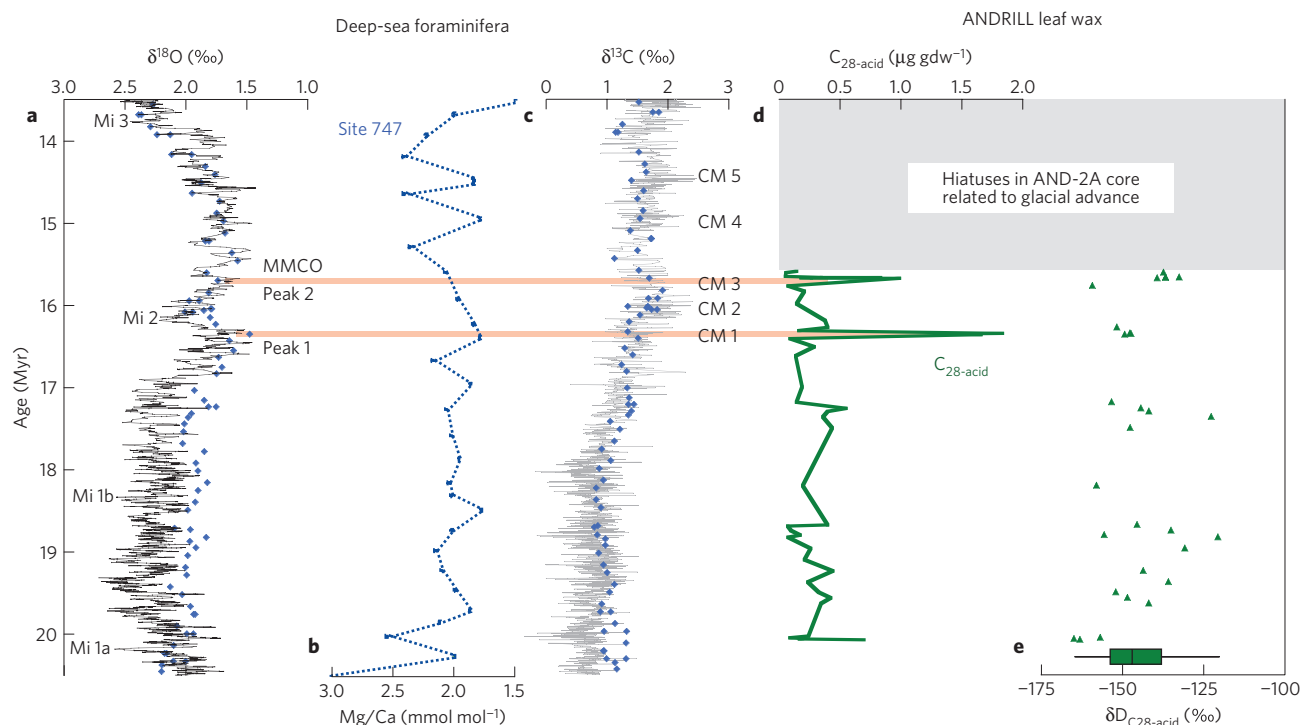


Figure 3 | Miocene climate records. **a**, Benthic stacked $\delta^{18}\text{O}$, five-point smooth⁴ (black); labelled warm events (Middle Miocene Climatic Optimum, MMCO, peak 1 and 2), and glacial events at marine isotope (Mi) stages 1–3 (ref. 1); Southern Ocean site 747 (ref. 4; blue). **b**, Southern Ocean site 747 Mg/Ca (ref. 1; blue). **c**, Benthic stacked $\delta^{13}\text{C}$ with five-point smooth⁴ (grey); $\delta^{13}\text{C}$ maxima (CM) 1–5 linked to productivity increases⁵; Southern Ocean site 747 (ref. 4; blue). **d**, Leaf-wax abundance. **e**, δD shown downcore (green) and δD summarized in box and whisker plot showing median (line), 75th and 25th percentiles (rectangle) and range (error bars). Pink shading as in Fig. 1; grey shading disrupted sedimentation.

Ross Sea in two brief pulses. Local optima 16.4 and 15.7 Myr ago (Fig. 3d) correspond to pulses of global warmth each <30,000 yr in duration identified in deep-sea archives within the generally warm middle Miocene⁴ (Fig. 3a). In the Ross Sea, temperate dinoflagellate species replace sea-ice indicator species and indicate sea surface temperatures in the range of 0–11.5 °C (Fig. 1c; ref. 3). Deep-ocean temperature reconstructions also show increased temperatures and reduced ice volumes throughout the middle Miocene¹ (Fig. 3) and model experiments suggest that global warmth was intensified at high latitudes⁹.

Our $\delta\text{D}_{\text{precip}}$ estimate of $\sim -50\text{‰}$ supports the multiproxy evidence for warmer temperatures at the Antarctic coast during the middle Miocene. However, other factors beyond temperature are known to influence water isotopes^{13,14} and the temperature versus δD slope (T – δD) in the Miocene could be different from today. Pairing proxy isotope data with isotope-enabled modelling is one effective way to identify competing dynamical influences on proxy isotopes²⁵. As there are no isotope-enabled general circulation models with realistic boundary conditions for the middle Miocene at present, we tested our results with an idealized grey-radiation aquaplanet moist general circulation model^{26,27} with the addition of isotopic tracers (iGRAM). Aquaplanet experiments provide reasonable constraints for the coastal site because precipitation isotopes at the margin of a continent are similar to the adjacent ocean⁶. Furthermore, iGRAM results match annual mean temperatures and precipitation isotopes by latitude compared with more complex realizations in the National Center for Atmospheric Research Community Atmosphere Model version 2 (ref. 6; Supplementary Fig. S2). Experiments with iGRAM include warm, ice-free conditions that provide physical and dynamical support for heavy polar precipitation isotopes (Supplementary Fig. S3). The model response of -51.4‰ for $+7.7\text{ °C}$ (at 77 °S) is quantitatively consistent with the leaf-wax result ($-51 \pm 3\text{‰}$). Critically, these model experiments

allow us to attribute our proxy-based observations to not only a temperature increase, but also to a less D -depleted atmospheric vapour source sustained by evaporation over the adjacent warmer oceans (Supplementary Table S3). The model–proxy combination allows us to infer that Miocene isotopes in precipitation reflect not just warmer temperatures, but also important changes in hydroclimate over the warmer Southern Ocean.

Both the modern Antarctic spatial T – δD relationship and a shallower slope based on our model experiments predict temperatures $>0\text{ °C}$ (Fig. 2). $\delta\text{D}_{\text{precip}}$ reconstructions are therefore consistent with pollen assemblage estimates of summer land surface temperatures of 0–10 °C (ref. 3). Our best estimate of summer (December–February) temperatures is $\sim 7\text{ °C}$ over Miocene vegetation versus -4 °C over the modern glaciated surface, although it remains an open question whether the warmth^{1,4} was sufficiently persistent throughout the middle Miocene to explain the long duration of increased $\delta\text{D}_{\text{precip}}$ values. Temperature inferences have uncertainties associated with topography, land cover and seasonality, not considered here; however, our results demonstrate that increased $\delta\text{D}_{\text{precip}}$ over Antarctica requires a high-latitude moisture source and warmer temperatures (Supplementary Table S3).

With the dynamical nature of the water isotope tracer in mind, we note that our leaf-wax-based $\delta\text{D}_{\text{precip}}$ reconstructions are similar to or higher than Arctic values reported during extreme greenhouse conditions¹⁹. The contrast in flora is dramatic between the tundra vegetation of the Miocene Antarctic and the tropical-type flora of the PETM Arctic²⁸; clearly temperatures alone cannot explain matching $\delta\text{D}_{\text{precip}}$ values. Instead, dynamics of water-vapour transport and rainout must explain the difference. For the Arctic, surrounded by land, surface ocean water became fresher during the PETM with lower δD (ref. 19) and convective rainfall may have generated D -depleted values at the extreme greenhouse

temperatures of the PETM (ref. 28). The similarity of δD values belies very different temperatures and hydrological processes.

For the middle Miocene, we find leaf-wax evidence for vegetation refugia on Antarctica with brief pulses of high pollen production. δD_{wax} values form the basis of palaeoprecipitation estimates that indicate warmer temperatures. D -enrichment also implies that the water-vapour source is close to the precipitation site⁶ and model experiments demonstrate that a warmer ocean would have supplied moisture to the atmosphere locally (42% sourced polewards of 75° S at 7.7°C), and increased rainfall on Antarctica. Relative to modern polar-desert conditions (at McMurdo station average temperature -16.9°C , precipitation 203 mm yr^{-1}) our findings suggest an intensified hydrological cycle consistent with evidence for tundra in the dry valleys of Antarctica²⁹. These exceptional reversals of past icehouse conditions may offer valuable insights into hydrological processes under future warming scenarios.

Methods

Data. Accompanying data can be found at: ftp://ftp.ncdc.noaa.gov/pub/data/paleo/contributions_by_author/feakins2012/feakins2012.txt, ftp://ftp.ncdc.noaa.gov/pub/data/paleo/contributions_by_author/feakins2012/feakins2012.xls.

Leaf-wax δD . Sediment samples (20 g) were processed to extract and purify leaf-wax n -alkanoic acids as described in detail elsewhere³⁰. δD values were analysed using a Thermo Scientific Trace gas chromatograph (ZB-5 ms column, $30\text{ m} \times 0.25\text{ mm} \times 1\text{ }\mu\text{m}$) with a programmable temperature vapourization injector operated in solvent-split mode connected through an Isolink pyrolysis furnace (at $1,420^\circ\text{C}$) to a Delta V Plus mass spectrometer. Peaks of hydrogen reference gas bracketed analytes, two of which were used for standardization of the isotopic analyses. Data were then normalized to the standard mean ocean water/standard light Antarctic precipitation isotopic scale by comparison with an external standard containing eight fatty acid methyl esters ($i\text{-C}_{14}$ to $i\text{-C}_{20}$; obtained from A. Schimmelmann, Indiana University, Bloomington) with δD values ranging from -167 to -231‰ . The accuracy of replicate analyses of the external standard was 4.4‰ (root mean square error, $n = 32$). The H_3 factor was determined daily averaging $6.056 \pm 0.125\text{ ppm mV}^{-1}$. The results are reported using conventional delta notation ($\delta D\text{‰}$).

Palynology. As in ref. 3.

Climate model experiment. See Supplementary Information.

Received 25 August 2011; accepted 15 May 2012; published online 17 June 2012

References

- Billups, K. & Schrag, D. P. Paleotemperatures and ice volume of the past 27 Myr revisited with paired Mg/Ca and O-18/O-16 measurements on benthic foraminifera. *Paleoceanography* **17**, 1003 (2002).
- Shevenell, A. E., Kennett, J. P. & Lea, D. W. Middle Miocene ice sheet dynamics, deep-sea temperatures, and carbon cycling: A Southern Ocean perspective. *Geochim. Geophys. Res.* **9**, Q02006 (2008).
- Warny, S. *et al.* Palynomorphs from a sediment core reveal a sudden remarkably warm Antarctica during the middle Miocene. *Geology* **37**, 955–958 (2009).
- Zachos, J. C., Pagani, M., Sloan, L., Thomas, E. & Billups, K. Trends, rhythms and aberrations in global climate 65 Myr to present. *Science* **292**, 686–692 (2001).
- Diester-Haass, L. *et al.* Mid-Miocene paleoproductivity in the Atlantic Ocean and implications for the global carbon cycle. *Paleoceanography* **24**, PA1209 (2009).
- Lee, J. E., Fung, I., DePaolo, D. J. & Otto-Bliesner, B. Water isotopes during the last glacial maximum: New general circulation model calculations. *J. Geophys. Res.* **113**, D19109 (2008).
- You, Y., Huber, M., Muller, R. D., Poulsen, C. J. & Ribbe, J. Simulation of the middle miocene climate optimum. *Geophys. Res. Lett.* **36**, L04702 (2009).
- Beerling, D. J. & Royer, D. L. Convergent Cenozoic CO_2 history. *Nature Geosci.* **4**, 418–420 (2011).
- Pagani, M. *et al.* The role of carbon dioxide during the onset of Antarctic glaciation. *Science* **334**, 1261–1264 (2011).
- Rignot, E. *et al.* Recent Antarctic ice mass loss from radar interferometry and regional climate modelling. *Nature Geosci.* **1**, 106–110 (2008).
- Anderson, J. B. *et al.* Progressive Cenozoic cooling and the demise of Antarctica's last refugium. *Proc. Natl Acad. Sci. USA* **108**, 11356–11360 (2011).
- Florindo, F., Harwood, D. M. & Levy, R. H. Introduction to Cenozoic Antarctic glacial history. *Global Planet. Change* **69** V–VII, <http://dx.doi.org/10.1016/j.gloplacha.2009.11.001> (2009).
- Masson-Delmotte, V. *et al.* A review of Antarctic surface snow isotopic composition: Observations, atmospheric circulation, and isotopic modeling. *J. Clim.* **21**, 3359–3387 (2008).
- Dansgaard, W. Stable isotopes in precipitation. *Tellus* **16**, 436–468 (1964).
- Petit, J. R. *et al.* Climate and atmospheric history of the past 420,000 years from the Vostok ice core, Antarctica. *Nature* **399**, 429–436 (1999).
- Jouzel, J. *et al.* Orbital and millennial Antarctic climate variability over the past 800,000 years. *Science* **317**, 793–796 (2007).
- Sugden, D. E. *et al.* Preservation of Miocene glacier ice in East Antarctica. *Nature* **376**, 412–414 (1995).
- Sachse, D. *et al.* Sources of variability in the hydrogen isotopic composition of organic compounds from photosynthetic organisms. *Annu. Rev. Earth Planet. Sci.* **40**, 221–249 (2012).
- Pagani, M. *et al.* Arctic hydrology during global warming at the Palaeocene/Eocene thermal maximum. *Nature* **442**, 671–675 (2006).
- Acton, G. *et al.* and The ANDRILL-SMS Science Team. Palaeomagnetism of the AND-2A Core, ANDRILL Southern McMurdo Sound Project, Antarctica. *Terra Ant.* **15**, 191–208 (2008–2009).
- Lewis, A. R., Marchant, D. R., Ashworth, A. C., Hemming, S. R. & Machlus, M. L. Major middle Miocene global climate change: Evidence from East Antarctica and the Transantarctic Mountains. *Geol. Soc. Am. Bull.* **119**, 1449–1461 (2007).
- Yang, H. *et al.* Carbon and hydrogen isotope fractionation under continuous light: Implications for paleoenvironmental interpretations of the High Arctic during Paleogene warming. *Oecologia* **160**, 461–470 (2009).
- Yang, H., Liu, W., Leng, Q., Hren, M. T. & Pagani, M. Variation in n -alkane [δ]D values from terrestrial plants at high latitude: Implications for paleoclimate reconstruction. *Org. Geochem.* **42**, 283–288 (2011).
- Jahren, A. H., Byrne, M. C., Graham, H. V., Sternberg, L. S. L. & Summons, R. E. The environmental water of the middle Eocene Arctic: Evidence from δD , $\delta \text{O-18}$ and $\delta \text{C-13}$ within specific compounds. *Paleogeogr. Paleoclimatol. Paleoeconol.* **271**, 96–103 (2009).
- Jouzel, J., Hoffmann, G., Koster, R. D. & Masson, V. Water isotopes in precipitation: Data/model comparison for present-day and past climates. *Quat. Sci. Rev.* **19**, 363–379 (2000).
- Frierson, D. M. W., Held, I. M. & Zurita-Gotor, P. A gray-radiation aquaplanet moist GCM. Part I: Static stability and eddy scale. *J. Atmos. Sci.* **63**, 2548–2566 (2006).
- O'Gorman, P. A. & Schneider, T. The hydrological cycle over a wide range of climates simulated with an idealized GCM. *J. Clim.* **21**, 3815–3832 (2008).
- Sluijs, A. *et al.* Subtropical arctic ocean temperatures during the Palaeocene/Eocene thermal maximum. *Nature* **441**, 610–613 (2006).
- Lewis, A. R. *et al.* Mid-Miocene cooling and the extinction of tundra in continental Antarctica. *Proc. Natl Acad. Sci. USA* **105**, 10676–10680 (2008).
- Tierney, J. E. *et al.* Northern hemisphere controls on tropical southeast African climate during the past 60,000 years. *Science* **322**, 252–255 (2008).

Acknowledgements

This research used samples acquired by the ANDRILL project and provided by the Antarctic Marine Geology Research Facility at Florida State University. The ANDRILL project is a multinational collaboration involving the Antarctic programmes of Germany, Italy, New Zealand and the USA. The Antarctic Marine Geology Research Facility is sponsored by the US National Science Foundation. Financial support for this research was provided by the US National Science Foundation (ANT-0342484 to D. Harwood and R. Levy, subawards 25-0550-0001-155 to S.J.F. and 25-0550-0001-137 to S.W., ANT-1048343 to S.W. and EAR-090919 to P. Molnar for J-E.L.). This material is based on work supported by the US National Science Foundation under cooperative agreement no. 0342484 through subawards administered and issued by the ANDRILL Science Management Office at the University of Nebraska-Lincoln, as part of the ANDRILL US Science Support program. Any opinions, findings, and conclusions or recommendations expressed in this material are those of the authors and do not necessarily reflect the views of the US National Science Foundation. We acknowledge laboratory assistance from M. Rincon, M. Cheetham, Z. Zhang and L. Foersterling and discussions with D. Harwood, A. Tripati, A. Kahmen, J. West, J. Tierney, P. Bart, R. Askin, H. Bao, A. Sessions, G. Schmidt and J. Hayes. The simulations were carried out on the Division of Geological and Planetary Sciences' Dell cluster at the California Institute of Technology, and J-E.L. thanks T. Schneider, T. Merlis, and Z. Tan for their help in incorporating isotopes into GRAM and support by the NASA ROSES Aura Science Team NNN07ZDA001N-AST07-0069.

Author contributions

S.J.F. conducted the organic geochemistry and δD analyses. S.W. directed the palynology. J-E.L. conducted the model experiments. S.J.F., S.W. and J-E.L. contributed to interpreting the data and writing the paper. All authors contributed to discussions of this work.

Additional information

The authors declare no competing financial interests. Supplementary information accompanies this paper on www.nature.com/naturegeoscience. Reprints and permissions information is available online at www.nature.com/reprints. Correspondence and requests for materials should be addressed to S.J.F.